Metabolic Engineering 81 (2024) 262–272

Contents lists available at ScienceDirect

Metabolic Engineering

journal homepage: www.elsevier.com/locate/meteng

Engineering 5-hydroxymethylfurfural (HMF) oxidation in *Pseudomonas* boosts tolerance and accelerates 2,5-furandicarboxylic acid (FDCA) production

Thorsten Lechtenberg, Benedikt Wynands, Nick Wierckx *

Institute of Bio- and Geosciences IBG-1: Biotechnology, Forschungszentrum Jülich, 52425 Jülich, Germany

ARTICLE INFO

Keywords:
5-(Hydroxymethyl)furfural (HMF)
2,5-Furandicarboxylic acid (FDCA)
Pseudomonas
Aldehyde stress
Periplasmic aldehyde oxidoreductase
Tolerance engineering

ABSTRACT

Due to its tolerance properties, *Pseudomonas* has gained particular interest as host for oxidative upgrading of the toxic aldehyde 5-hydroxymethylfurfural (HMF) into 2,5-furandicarboxylic acid (FDCA), a promising biobased alternative to terephthalate in polyesters. However, until now, the native enzymes responsible for aldehyde oxidation are unknown. Here, we report the identification of the primary HMF-converting enzymes of *P. taiwanensis* VLB120 and *P. putida* KT2440 by extended gene deletions. The key players in HMF oxidation are a molybdenum-dependent periplasmic oxidoreductase and a cytoplasmic dehydrogenase. Deletion of the corresponding genes almost completely abolished HMF oxidation, leading instead to aldehyde reduction. In this context, two HMF-reducing dehydrogenases were also revealed. These discoveries enabled enhancement of *Pseudomonas'* furanic aldehyde oxidation machinery by genomic overexpression of the respective genes. The resulting BOX strains (Boosted OXidation) represent superior hosts for biotechnological synthesis of FDCA from HMF. The increased oxidation rates provide greatly elevated HMF tolerance, thus tackling one of the major drawbacks of whole-cell catalysis with this aldehyde. Furthermore, the ROX (Reduced OXidation) and ROAR (Reduced Oxidation And Reduction) deletion mutants offer a solid foundation for future development of Pseudomonads as biotechnological chassis notably for scenarios where rapid HMF conversion is undesirable.

1. Introduction

Non-pathogenic soil dwelling bacteria of the *Pseudomonas* clade, such as the aspiring biotechnological workhorses *P. putida* KT2440 and *P. taiwanensis* VLB120, show highly developed native tolerance traits towards various toxicants and are therefore promising starting points for the engineering of novel chassis strains with superior stress resistance (Bitzenhofer et al., 2021; Mukhopadhyay, 2015). This tolerance extends to aldehydes (Bitzenhofer et al., 2021) which, despite numerous possible applications enabled by their versatile reactivity, remain challenging for whole-cell biocatalytic processes (Zhou et al., 2020). Aldehydes are potent electrophiles and easily undergo addition reactions with various biogenic nucleophiles like amino or thiol functionalities of proteins or nucleic acids, which can result in severe cell damage through misfolding and crosslinking (Lee and Park, 2017; LoPachin and Gavin, 2014). Consequently, living systems endeavor to avoid the presence of aldehydes and rapidly convert them to the less noxious alcohol or carboxylic acid derivatives (Wierckx et al., 2011). While many microbes, such as *Escherichia coli*, *Corynebacterium glutamicum* or *Saccharomyces cerevisiae* depend on energy-consuming alcohol formation, *P. putida* KT2440 preferentially uses oxidative aldehyde detoxification (Fig. 1A) (Kim et al., 2022; Kunjapur et al., 2014; Wang et al., 2018; Xu et al., 2020b). Their capability to rapidly oxidize aldehydes, along with their outstanding tolerance properties, renders Pseudomonads particularly attractive for whole-cell biocatalytic production of terephthalate-substituting plastic monomer FDCA from HMF (Troiano et al., 2020; Yuan et al., 2020). Together with ethylene glycol, FDCA can be used to synthesize the fully biobased and performance-advantaged polymer polyethylene furanoate (PEF) that features better barrier, thermal and mechanical qualities than conventional polyethylene terephthalate (PET) (Davidson et al., 2021; Loos et al., 2020).

Listed among the revised top chemical opportunities from biorefinery carbohydrates and often described as "Sleeping Giant" of sustainable chemistry, HMF, the dehydration product of hexoses, represents an industrially relevant model aldehyde that can be converted into a wide range of high-value products including FDCA (Bozell

* Corresponding author. Wilhelm-Johnen-Str., Building 15.4, Room 13352425 Jülich, Germany
E-mail addresses: t.lechtenberg@fz-juelich.de (T. Lechtenberg), b.wynands@fz-juelich.de (B. Wynands), n.wierckx@fz-juelich.de (N. Wierckx).

https://doi.org/10.1016/j.ymben.2023.12.010
Received 26 October 2023; Received in revised form 12 December 2023; Accepted 21 December 2023
Available online 26 December 2023

and Petersen, 2010; Galkin and Ananikov, 2019; van Putten et al., 2013; Xu et al., 2020a). The oxidative cascade for the bioproduction of the dicarboxylic acid from HMF involves three sequential steps-including two aldehyde and one alcohol oxidation, resulting in the intermediates 5-hydroxymethyl-2-furoic acid (HMFA) and 5-formyl-2--furoic acid (FFA). The first whole-cell biocatalyst efficiently producing highly pure FDCA from HMF was described in 2010, using *P. putida* S12 expressing the alcohol oxidase *hmfH* from the HMF-degrading bacterium *Cupriavidus basilensis* (Koopman et al., 2010a, 2010b). This strain was subsequently improved by additional expression of an aldehyde dehydrogenase (ALDH) and the transporter *hmfT1* (Pham et al., 2020; Wierckx et al., 2015). Other examples comprising bacteria of the *Pseudomonas* clade for FDCA production employed either a different alcohol oxidase, a co-cultivation strategy, or a hybrid process combining whole-cell catalysis with purified enzymes (Hsu et al., 2020; Lin et al., 2020; Tan et al., 2020; Zou et al., 2020). Moreover, a few other species,

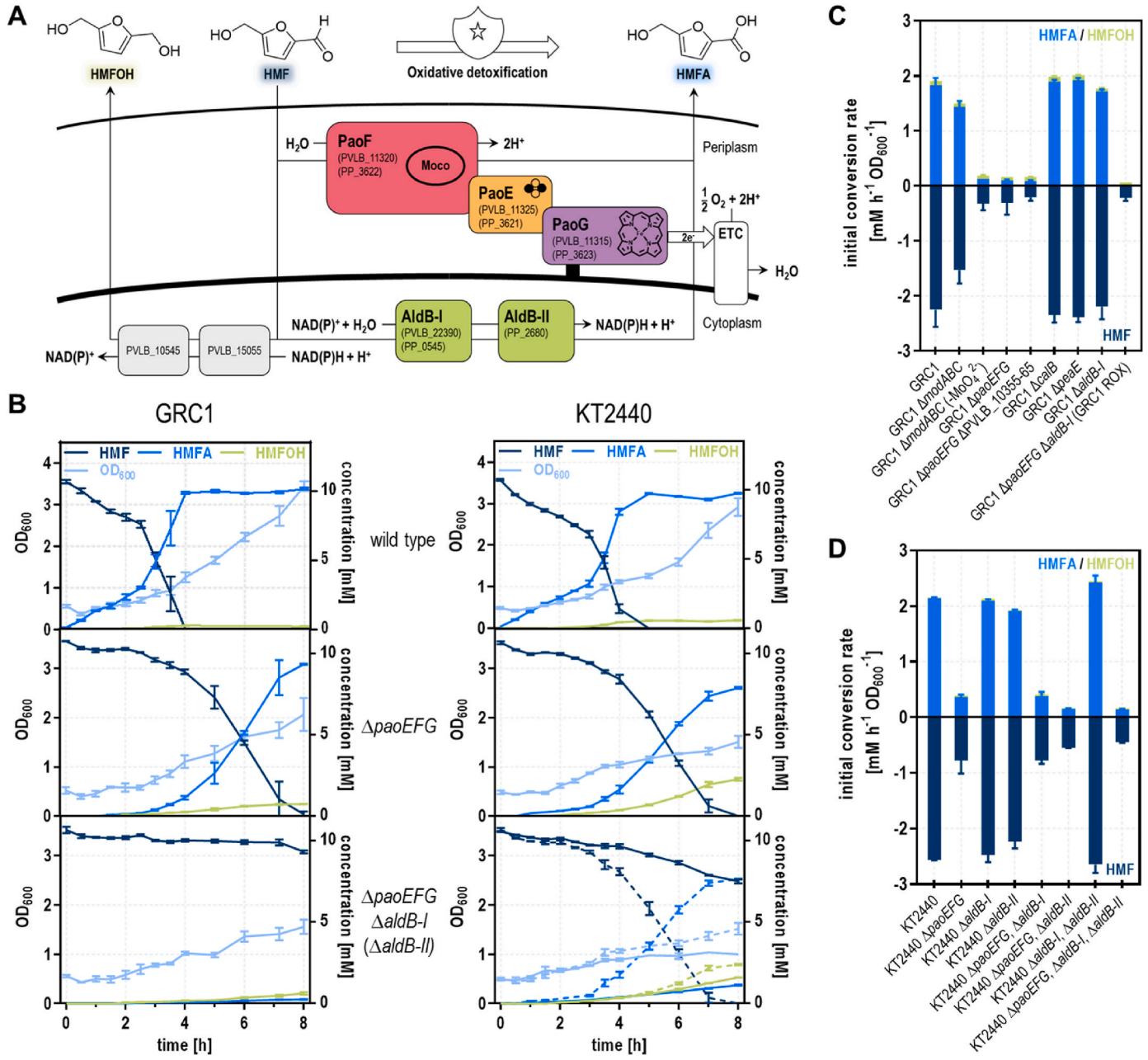

Fig. 1. HMF conversion by the biotechnological workhorses *P. taiwanensis* VLB120 GRC1, *P. putida* KT2440 and deletion mutants thereof unveiling the enzymes involved in this process. (**A**) Reaction scheme depicting oxidative and reductive detoxification of HMF to HMFA and HMFOH. (**B**) HMF conversion in 24-deepwell microplates (two-fold buffered MSM with 40 mM glycerol, 2 mM glucose, and 10 mM HMF) using whole-cells of GRC1 and KT2440 compared to derived Δ*paoEFG* and Δ*aldB-I(I)* mutants. In the bottom graph of the KT2440 panel, dotted lines correspond to the double mutant KT2440 Δ*paoEFG* Δ*aldB-I* and solid lines to the triple mutant KT2440 Δ*paoEFG* Δ*aldB-I* Δ*aldB-II*. Error bars represent the mean ± standard deviation of three replicates. (**C**) Initial HMF depletion, as well as HMFA and HMFOH formation rates of GRC1 and selected mutant strains thereof in shake flasks. The data presented include the mean and standard error of at least two independent experiments each performed in duplicates. Full reaction courses are provided in the Supporting Information (Fig. S2). In case of a single dataset (GRC1 Δ*calB*, GRC1 Δ*peaE,* and GRC1 Δ*aldB-I*), the error bars correspond to the standard error of the slope of the linear regression. (**D**) Initial HMF depletion, as well as HMFA and HMFOH formation rates of KT2440 and selected mutant strains thereof in 24-deepwell microplates. The data presented include the mean and standard error of two independent experiments each performed in triplicates. Full reaction courses are provided in the Supporting Information (Fig. S3). Abbreviation: ETC, electron transport chain.

such as *Raoultella ornithinolytica* BF60, were also applied to produce FDCA from HMF (Hossain et al., 2017; Sayed et al., 2022; Sheng et al., 2020; Yuan et al., 2018).

Despite the extensive exploitation of *Pseudomonas*' native oxidative features, the enzyme(s) actually responsible for aldehyde detoxification remained unknown (Liu et al., 2020). The presence of many genes encoding ALDHs (32 for *P. putida* KT2440 and 25 for *P. taiwanensis* VLB120, Table S1) and numerous other putative aldehyde-converting oxidoreductases makes identifying these enzymes like a search for a needle in the haystack. Zheng et al. demonstrated that HMF oxidation of *P. putida* KT2440 was heavily affected by the deletion of the molybdate uptake system *modABC* (Zheng et al., 2020). This is in accordance with findings attributing a pivotal role to at least one molybdenum-dependent enzyme for the transformation of other aromatic aldehydes like vanillin, *p*-anisaldehyde, and piperonal (Adewunmi et al., 2020; Doi et al., 2016; Graf and Altenbuchner, 2014; Kozono et al., 2020). The PaoABC enzyme from *E. coli* is a well-described bacterial aldehyde-oxidizing enzyme depending on a molybdenum cofactor. It belongs to the xanthine oxidase family and is a periplasmic heterotrimer which consists of a large molybdenum-dependent subunit, a medium-size FAD-containing subunit and a small subunit harboring two iron-sulfur clusters (Correia et al., 2016; Neumann et al., 2009). *In vitro* experiments with purified enzyme proved a wide substrate spectrum of multiple mostly aromatic aldehydes including HMF and FFA (McKenna et al., 2017; Neumann et al., 2009). In an enzymatic cascade with a galactose oxidase variant, PaoABC was also successfully used to synthesize FDCA from HMF (McKenna et al., 2017).

In this work, we investigated the enzymatic furanic-aldehyde oxidation toolbox of *P. taiwanensis* VLB120 and *P. putida* KT2440. Consecutive gene deletions revealed a crucial role of a so far uncharacterized periplasmic molybdenum-dependent enzyme complex that is complemented by one or more cytoplasmic ALDHs. Strains deprived of their oxidation ability showed higher susceptibility to HMF and increased aldehyde reduction occurred as secondary tolerance mechanism, and we identified the main HMF-reducing enzymes. Overexpression of the newly discovered enzymes led to higher HMF tolerance through redox detoxification, while also enhancing FDCA production. Hence, this work uncovers the interplay between aldehyde oxidation and tolerance, highlighting the periplasm as first line of defense in catalytic tolerance mechanisms.

2. Results and discussion

2.1. Identification of HMF-oxidizing enzymes in P. taiwanensis VLB120 and P. putida KT2440

The HMF-oxidizing properties of *P. taiwanensis* VLB120 and *P. putida* KT2440 were evaluated and shown to be very similar (Fig. 1B). Therefore, we expected both organisms to be equipped with a comparable set of aldehyde-converting enzymes and thus searched for candidates with homologs in both species. This excluded the PaoABC homolog of *P. putida* KT2440 since it is absent in *P. taiwanensis* VLB120. Additionally, the *P. putida* enzyme (PP_3308-10) lacks a TAT signal sequence unlike that of *E. coli*, which presumably prevents its export into the periplasm (Fig. S1). BLAST analysis revealed several related molybdenum-dependent enzymes as candidates for HMF oxidation in both species (Fig. S1). Since we had a genome-reduced chassis (GRC1) (Wynands et al., 2019) with improved process and tolerance features at hand and found only two promising operons in this strain, we decided to first elucidate HMF oxidation in *P. taiwanensis* VLB120. Initially, we verified the importance of one or more molybdenum-dependent enzyme (s) by deletion of the molybdate transporter system *modABC* in GRC1. Surprisingly, oxidation rates were only slightly affected under standard assay conditions, at first glance contradicting previous findings for *P. putida* KT2440 (Graf and Altenbuchner, 2014; Zheng et al., 2020). However, our minimal salts medium (MSM) contains 0.2 mg L^{-1} $Na_2MoO_4 \times 2H_2O$, which could be higher than the concentration in previously tested media such as the lysogeny broth (LB) used by Zheng et al. This may mask transport effects. Indeed, upon omission of this molybdenum source from the medium the initial oxidation rates of GRC1 Δ*modABC* were heavily impaired compared to the wild type, confirming the involvement of at least one molybdenum-dependent enzyme in HMF detoxification by *P. taiwanensis* VLB120 (Fig. 1C, Fig. S2).

The two operons encoding putative molybdenum-depending enzymes identified by BLAST analysis (Fig. S1) are designated by the locus tags PVLB_11305-PVLB_11325 and PVLB_10350-PVLB_10365. In both cases the molybdopterin-binding subunit harbors a putative TAT signal and shares a little more than 25% amino acid sequence similarity with PaoC (Fig. S1). In contrast to PaoABC, the third subunit is not FAD-binding, but a cytochrome according to *in silico* predictions (Winsor et al., 2016). The PVLB_11305-PVLB_11325 cluster additionally encodes a chaperone resembling PaoD and a MobA-like transferase that is probably involved in molybdopterin cofactor (Moco) biosynthesis. We deleted the three catalytically relevant genes of this cluster and observed an 86% drop of initial HMF conversion rates similar to that of the transporter-deficient strain establishing an important function of this periplasmic molybdenum-dependent enzyme in HMF detoxification of *P. taiwanensis* VLB120 (Fig. 1). The newly discovered enzyme complex was named PaoEFG (Fig. 1A).

The *paoEFG* deletion reduced initial HMF oxidation considerably, but rates increased after 4 h and the mutant still completely converted the aldehyde in about 8 h. Consequently, at least one more enzyme is involved in the process and the delayed activity points to inducible expression (Fig. 1B). A participation of the second putative molybdenum-dependent oxidoreductase PVLB_10350-65 was excluded, since a double deletion mutant displayed the same oxidation rate as the single Δ*paoEFG* strain (Fig. 1C, Fig. S2). Therefore, we switched our focus to the plethora of predicted ALDHs (Table S1). Based on presence in both *P. taiwanensis* VLB120 and *P. putida* KT2440 and annotations related to aromatic aldehydes, *calB* (PVLB_01470, putative coniferyl aldehyde dehydrogenase), *peaE* (PVLB_12825, putative phenylacetaldehyde dehydrogenase) and *aldB-I* (PVLB_22390, putative aldehyde dehydrogenase B) were chosen for deletion. The initial HMF conversion rates were slightly reduced for GRC1 Δ*aldB-I* (Fig. 1C, Fig. S2). Thus, we generated the double deletion mutant GRC1 Δ*paoEFG* Δ*aldB-I*. This strain (hence called GRC1 ROX for Reduced OXidation) showed only marginal HMF oxidation activity producing less than 1 mM HMFA from 10 mM HMF in 24 h (Fig. 1B and C, Fig. S2). Accordingly, *P. taiwanensis* VLB120 has two main HMF oxidizing enzymes. In our setup with externally added aldehyde, PaoEFG likely represents the primary defense system because its deletion had the most drastic effect. Theoretically, periplasmic oxidation of HMF would avoid its toxic effects inside the cell. In this proposition, AldB-I provides a second line of defense by detoxifying aldehyde molecules which pass this first barrier.

Both species analyzed in this study share high similarity, but also have a few conspicuous differences, such as the absence of the *ped*-cluster in *P. taiwanensis* VLB120, which among others contains several highly expressed alcohol and aldehyde dehydrogenases (*pedE*, *pedH*, *pedI*) (Li et al., 2020; Wehrmann et al., 2020; Winsor et al., 2016). We therefore investigated whether the results obtained for *P. taiwanensis* VLB120 could be transferred to the currently still more widely used *P. putida* KT2440. This strain harbors homologs to the newly identified *paoEFG* (PP_3621-23) and AldB-I (PP_0545), both with amino acid sequence similarities greater than 90% (Fig. S1). As expected, deletion of the *paoEFG* operon led to a similar HMF oxidation deficiency as observed for GRC1 (Fig. 1B and D, Fig. S3). However, a higher residual activity remained upon additional deletion of AldB-I (PP_0545). This activity was further reduced by deletion of AldB-II (PP_2680, 87% identity to AldB-I from *P. taiwanensis*) also known as PedI (Table S1), although the residual HMF oxidation activity was still slightly higher than that of GRC1 ROX (Fig. 1B and D, Fig. S3). In *P. putida* KT2440

AldB-II seems to be more important than AldB-I since, in the *ΔpaoEFG* background, *aldB-I* deletion had little effect while *aldB-II* deletion yielded a lower activity (Fig. 1D, Fig. S3).

2.2. Identification of HMF-reducing enzymes in P. taiwanensis VLB120

Following the elucidation of the enzymatic toolbox for oxidative HMF detoxification, we aimed at discovering *Pseudomonas*' furanic aldehyde reduction machinery, which was focused on *P. taiwanensis* VLB120 GRC1 due to its potential process-oriented advantages (Wynands et al., 2019). In the ROX strain, about half of the HMF was reduced to 5-hydroxymethylfurfuryl alcohol (HMFOH) (Fig. S2) proving that *P. taiwanensis* VLB120 can use HMF reduction as alternative detoxification pathway. Diol formation is of biotechnological interest as well, because, like FDCA, HMFOH can serve as a symmetrical monomer for the production of plastics (Wu et al., 2023). Inspired by the *E. coli* RARE strain designed by the Prather lab (Kunjapur et al., 2014), we undertook to minimize HMF conversion. For this, we searched for homologs of the aldo-keto reductases (AKRs) (*dkgB*, *yeaE*, *dkgA*) and alcohol dehydrogenases (ADHs) (*yqhD*, *yahK*, *yjgB*) responsible for benzaldehyde reduction by *E. coli* (Kunjapur et al., 2014). The three most similar AKRs and ADHs (PVLB_10970, PVLB_11635, PVLB_14845, PVLB_10545, PVLB_15055, PVLB_22390) were knocked out in GRC1 ROX (Table S2). Since HMF reduction was much slower than oxidation, cultivation time was prolonged to about 2 days, which allowed better detection of small differences in HMFOH formation. Remarkably, only removal of PVLB_10545 coding for an enzyme annotated as ethanol-active dehydrogenase/acetaldehyde-active reductase (AdhP) (www.pseudomonas.com (Winsor et al., 2016)) lowered HMFOH formation significantly by about 40 % (Fig. 2). A second set of deletion mutants using GRC1 ROX Δ*adhP* (ΔPVLB_10545) as new background revealed that PVLB_15055 also contributed to a small but significant extent as the respective mutant produced about 13% less HMFOH compared to the Δ*adhP* reference (Fig. 2). Since its counterpart in *P. putida* KT2440 (PP_2426) has recently been proven responsible for vanillin reduction, we had assumed a more serious impact (Garcia-Hidalgo et al., 2020). The knockout of the other four tested genes did not significantly ($p > 0.01$) alter HMFOH production (Fig. 2). Nevertheless, we could identify AdhP and the ADH tagged PVLB_15055 as important

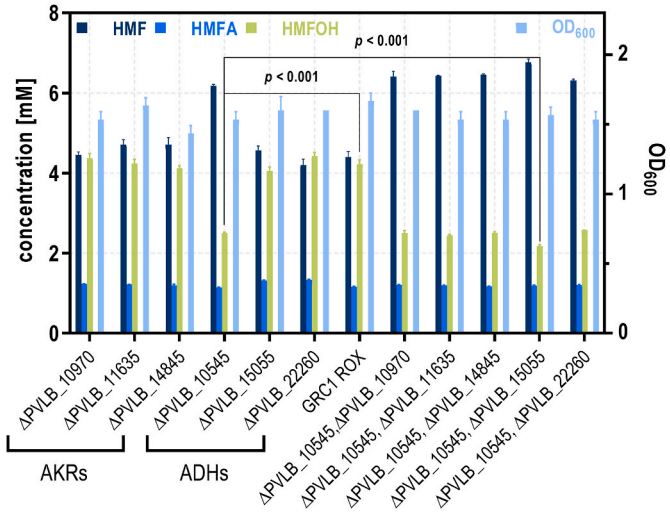

Fig. 2. Tracing of HMF-reducing enzymes in *P. taiwanensis* VLB120 GRC1. Final furanics concentrations and OD_{600} of HMF conversion assays in shake flasks (four-fold buffered MSM with 40 mM glycerol, 2 mM glucose, and 10 mM HMF) using whole-cells of GRC1 ROX and derived deletion mutants lacking putative AKRs and ADHs. Samples were taken after 51 h. The mean and standard deviation of three replicates is shown. *P* values were calculated by two-tailed Student's *t*-tests.

members of GRC1's toolset for reductive HMF detoxification accounting for about half of the alcohol formation.

In all, the redox-neutralized GRC1 Δ*paoEFG* Δ*aldB-I* Δ*adhP* ΔPVLB_15055 (GRC1 ROAR, Reduced Oxidation And Reduction, named according to a previously published *E. coli* variant with similar properties (Butler et al., 2023)) only metabolized HMF at an average rate of 47 ± 1 μM h^{-1} OD_{600}^{-1}, which is more than 40-fold slower than the GRC1 parent strain. Next to GRC1 ROX, it thus constitutes a promising novel chassis for redox-sensitive applications, for example future investigation of further HMF tolerance mechanisms which, in the wild type background, might be masked by predominant rapid oxidation. Moreover, if follow-up work can demonstrate, as observed for *Ec*PaoABC (Neumann et al., 2009), that the substrate spectrum of PaoEFG and the other identified enzymes includes additional aromatic aldehydes besides HMF, *Pseudomonas* strains with reduced oxidation and reduction properties can turn into alternative platforms for the microbial production of valuable aldehydes or aldehyde-derived compounds (Kunjapur and Prather, 2015; Zhou et al., 2020).

2.3. PaoEFG and AldB-I are crucial for tolerance towards HMF

It is generally implied that oxidation and reduction of aldehydes are a major mechanism to abate their toxic effect, but this tolerance mechanism was until now not quantitatively investigated. We therefore assessed the importance of oxidative aldehyde detoxification for the viability of GRC1 in presence of HMF as a stressor. The oxidation-deficient strains were exposed to increasing concentrations of the toxic aldehyde and cell growth was monitored. The deletion mutants grew identically to the unmodified GRC1 in the absence of aldehyde stress, but showed notably prolonged lag phases when HMF was added (Fig. 3). Remarkably, the severity of the growth impairment followed exactly the oxidation capacity, indicating a cumulative effect of the two oxidoreductases on HMF tolerance.

In strains capable of detoxifying HMF in the periplasm, deletion of the cytoplasmic dehydrogenase *aldB-I* had only marginal influence on aldehyde conversion rates, and a retarded growth of the deletion mutant only became apparent at 20 mM HMF (Fig. 3). This indicates that PaoEFG can convert modest concentrations of the externally supplemented toxic aldehyde in the periplasm prior to its entry into the cell. Only at higher HMF concentrations is this first barrier breached, at which point the advantage of the cytoplasmic AldB-I manifests. In contrast, when GRC1 was deprived of its periplasmic detoxification mechanism, growth was already considerably impaired at 10 mM HMF and completely suppressed at concentrations above 15 mM (Fig. 3). The double deletion mutant GRC1 ROX performed even worse and growth in presence of 10 mM HMF only occurred after a lag phase of more than four days (Fig. 3). Under the tested conditions, these results corroborate the central role of PaoEFG for HMF tolerance, which heavily depends on fast aldehyde conversion. Furthermore, it can be concluded that cytoplasmic HMF oxidation by AldB-I can partially compensate lacking periplasmic detoxification, but it is not as efficient. This fits perfectly with the previously determined conversion rates and supports the theory that periplasmic oxidation is better than cytoplasmic oxidation for ameliorating HMF toxicity.

2.4. Tolerance engineering enables GRC1 to withstand higher HMF concentrations

Since disruption of the HMF-converting enzymes of *P. taiwanensis* VLB120 increased sensitivity towards the furanic aldehyde, we hypothesized that their overexpression would increase HMF tolerance. For this purpose, we employed the BacPP (de Avila et al., 2011) tool to identify the native promoter sequences of the *paoEFGHI* operon and *aldB-I* (Fig. S4). Expression of *paoEFGHI* and *aldB-I* was predicted to be controlled by stress-induced σ^{38}-promoters, which we substituted by the strong and constitutive P_{14f} promoter (Zobel et al., 2015). Commonly,

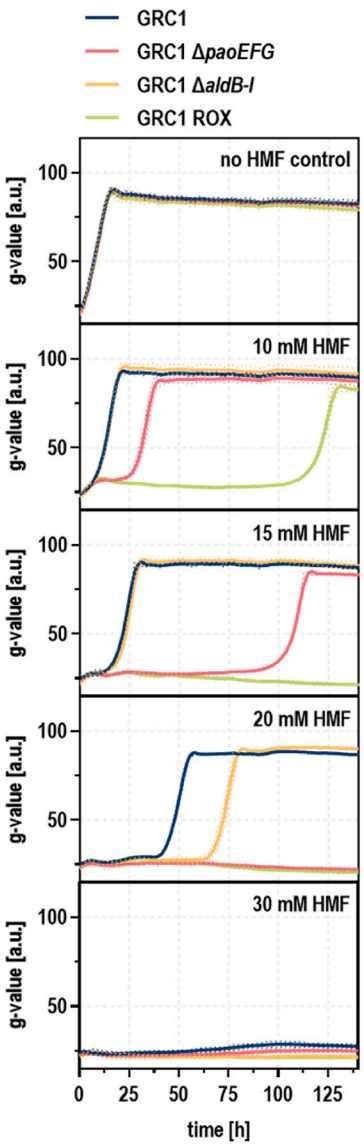

Fig. 3. Importance of aldehyde oxidation for HMF tolerance. Four-fold buffered MSM supplemented with 40 mM glycerol and 2 mM glucose as carbon sources and increasing HMF concentrations was inoculated with the unmodified GRC1 (blue), the single deletion mutants GRC1 Δ*paoEFG* (red), GRC1 Δ*aldB-I* (yellow) and the double deletion mutant GRC1 ROX (green) to an OD_{600} of 0.1. Cells were cultivated in a Growth Profiler in 96-well microtiter plates. The growth curves result from a second-order smoothing to the mean values obtained from three replicates. The dots represent the standard deviation.

this synthetic promoter is used together with a downstream BCD2 element encoding a short leader peptide which reduces gene-specific translation effects and increases expression levels (Mutalik et al., 2013), but introduction of this extended promoter sequence led to suppressor mutations indicating that the high expression of the *paoEFGHI* cluster was too stressful for the cells. Reasons for this could be the biochemically complex Moco synthesis, an extensive demand for iron required for the cytochrome and the iron-sulfur clusters, or most likely membrane destabilization caused by intensive transport of folded proteins into the periplasm through the TAT system. This is supported by the fact that a similar promoter replacement with P_{14f} BCD2 for *aldB-I*, encoding the simpler cytoplasmic dehydrogenase, was successfully implemented (Fig. 4A). To attenuate the expression level, we generated alternative constructs omitting the translational coupler and keeping the native ribosome-binding sites (RBS) instead (Fig. 4A). In this case, correct clones were obtained as verified by Sanger sequencing. To further reduce metabolic burden, another strain was generated using the weaker P_{14c} promoter to control *paoEFGHI* expression. The resulting GRC1 BOX-C/P strains (Boosted OXidation in the cytoplasm (C) and/or periplasm (P)) were tested for their ability to oxidize HMF.

Strikingly, both the exchange to the moderately strong P_{14c} promoter and to the strong P_{14f} promoter upstream of the *paoEFGHI* cluster (BOX-P1 and BOX-P2) resulted in a more than five-fold increase in initial HMF conversion rates (Fig. 4B). This allowed the complete detoxification of 10 mM HMF to HMFA in less than 2 h when using a comparatively low starting OD_{600} of 0.5 (Fig. S5). In contrast to this, exchange of the *aldB-I* promoter affected aldehyde detoxification to a lesser extent. While BOX-C2 harboring the extended promoter sequence including BCD2 showed at least a doubling of the initial HMF oxidation rate, BOX-C1 possessing the native RBS only exhibited marginally improved oxidative properties (Fig. 4B). These findings are in accordance with the results obtained for the deletion mutants highlighting that periplasmic oxidation is clearly more efficient than the cytoplasmic reaction catalyzed by AldB-I. In this setting, with 10 mM externally supplemented HMF, oxidation rates were not further increased when *paoEFGHI* and *aldB-I* were simultaneously overexpressed. For BOX-C2P2 we even observed a slight deterioration which can presumably be attributed to an increased metabolic burden, since this strain also grew slightly slower without HMF (Fig. 4B and C). We hypothesized that with 10 mM HMF higher turnover rates were not possible due to substrate limitation, possibly caused by gradient-driven import into the cytoplasm. This was confirmed by cultures with 25 and 40 mM HMF, where BOX-C2P2 performed best (Fig. 4D and E). Under these conditions, when a lower cell density faced a higher HMF concentration, a differentiation occurred exactly as anticipated according to the relative importance of the two oxidoreductases and chosen promoter strengths. In contrast to oxidation rates determined with 10 mM HMF, weaker expression of *paoEFGHI* in BOX-P1 led to worse growth with 25 mM HMF compared to BOX-P2. However, the strain still performed slightly better than BOX-C2 which solely relied on maximum expression of *aldB-I*. The hierarchy became even more pronounced when the HMF concentration was increased to 40 mM. In this case, GRC1 and BOX-C1 were no longer able to grow at all within the observation period, while all BOX strains headed by BOX-C2P2 withstood the high concentration of the toxicant (Fig. 4E). Analysis of HMF and HMFA concentrations during growth experiments in presence of 25 mM aldehyde confirmed rapid oxidation as primary tolerance mechanism (Fig. 4F). BOX-C2P2 equipped with the maximum amount of HMF-oxidizing enzymes showed fastest oxidation during the lag phase with ten-fold higher initial HMF conversion compared to the unmodified GRC1. The detoxification rates of the other strains also corresponded exactly to their growth performance (Fig. 4B, D, F).

In conclusion, the constitutive overexpression of *paoEFG* and *aldB-I* prepared the bacteria for growth under HMF stress, which is essential for competitive industrial bioprocesses involving this toxic aldehyde. Certainly, expression of the oxidoreductases will also be inherently induced upon exposure to the toxicant, which can be seen by increasing oxidation rates of the strains over time (Fig. 1B). Nevertheless, the primary effect of furanic aldehyde stress is a prolongation of the lag phase (Heer and Sauer, 2008), and the BOX strains are thus primed for HMF detoxification at the most critical time for tolerance, the initial stage of growth. Similarly, a previous study demonstrated that a constitutive solvent-tolerant strain (permanently expressing the efflux pump *ttgGHI*) exhibited superior growth properties than one with natural regulation when exposed to 4-ethylphenol as a stressor (Wynands et al., 2019). Additionally, handling becomes significantly simplified as the need for induction is eliminated. This is particularly advantageous in the case of HMF, where the inducer is continuously converted.

2.5. Optimized FDCA production

After identification of *paoEFG* and *aldB-I* as major genes for defense

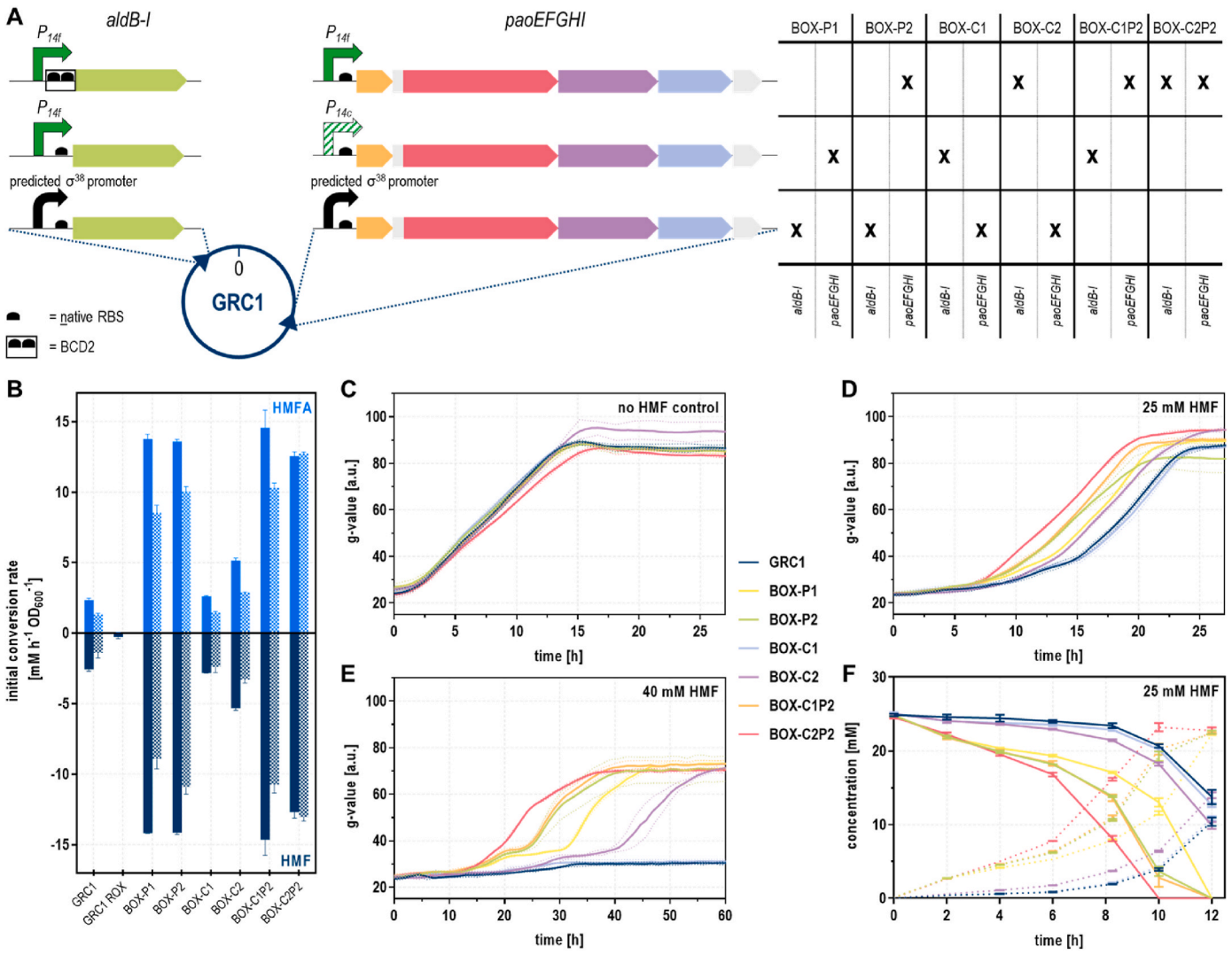

Fig. 4. Chromosomal overexpression of *paoEFGHI* and *aldB-I* enhances the oxidation ability of *P. taiwanensis* VLB120 GRC1 and leads to improved HMF tolerance. (**A**) Genomic composition of the respective genes. Expression is modified by replacing the predicted native σ^{38} promoters with different strong and constitutively active ones. An overview of all combinations of promoter exchanges and their respective genotypes is given in the enclosed table. (**B**) Initial HMF depletion and HMFA formation rates of GRC1, GRC1 ROX as negative control, and the generated promoter exchange mutants. Filled bars show the mean and standard error of two independent experiments in 24-deepwell microplates (two-fold buffered MSM with 40 mM glycerol, 2 mM glucose, 10 mM HMF, starting $OD_{600} = 0.5$) each performed in triplicates. Full reaction courses are provided in the Supporting Information (Fig. S5). Shaded bars indicate the initial conversion rates of the growth experiment depicted in panel **D** and **F** (25 mM HMF, starting $OD_{600} = 0.1$) determined by linear regression limited to the first 6 h. The OD_{600} was assumed constant during this period and equaled the starting conditions. The error bars correspond to the standard error of the slope of the linear regression. Growth of the promoter exchange mutants (two-fold buffered MSM with 40 mM glycerol and 2 mM glucose) and the unmodified GRC1 without HMF (**C**) and with 25 mM (**D**) and 40 mM (**E**) HMF. Experiments were carried out in a Growth Profiler and growth curves result from a second-order smoothing to the mean values obtained from three replicates. The dots represent the standard deviation. (**F**) HMF (solid lines) and HMFA (dotted lines) concentrations observed during the growth experiments in presence of 25 mM HMF. The mean and standard deviation of three replicates is shown.

against HMF and optimization of their expression which resulted in markedly improved oxidation rates and tolerance, we hypothesized that the new BOX strains could also produce FDCA more efficiently. The oxidoreductase HmfH is needed to oxidize the hydroxy group of HMFA (Koopman et al., 2010a; Pham et al., 2020), while the HmfT transporter improves FDCA production likely by facilitating HMFA uptake (Pham et al., 2020; Wierckx et al., 2015). Starting from HMFA, the further reaction pathway then proceeds via FFA, another aldehyde, which was previously shown to be oxidized by *Pseudomonas* (Tan et al., 2020), ultimately yielding the dicarboxylic acid FDCA (Fig. 5A). Both heterologous genes required are part of the *hmf*-cluster enabling microbial growth on furanic aldehydes HMF and furfural (Koopman et al., 2010b). In this study, *Paraburkholderia caribensis*, which can grow on both aldehydes as sole carbon and energy source (data not shown), was chosen as donor strain for the mentioned genes (Achouak et al., 1999). Using a *tac*-promoter, which is constitutive in *Pseudomonas* lacking the *lacI* repressor, strong *hmfH* expression was achieved with plasmid pBT'T_*hmfH*. In contrast, excessive presence of transporter proteins negatively influences the cell's fitness due to membrane destabilization. Therefore, expression of *hmfT* was set under the control of the salicylate-inducible *nagR/*P_{nagAa} promoter on the lower-copy plasmid pJNN_*hmfT*. The resulting series of FDCA-producing strains is denoted as BOX-C/P-*hmfH-hmfT*. The heterologous expression of *hmfH* led to formation of FDCA in all tested strains and the beneficial role of the HmfT transporter was confirmed because induction of P_{nagAa} with 100 μM salicylate considerably improved production in all cases (Fig. 5, Fig. S6). The BOX-C2P2-*hmfH-hmfT* strain with maximized oxidation capacity significantly out-performed the GRC1 control, proving the benefit of

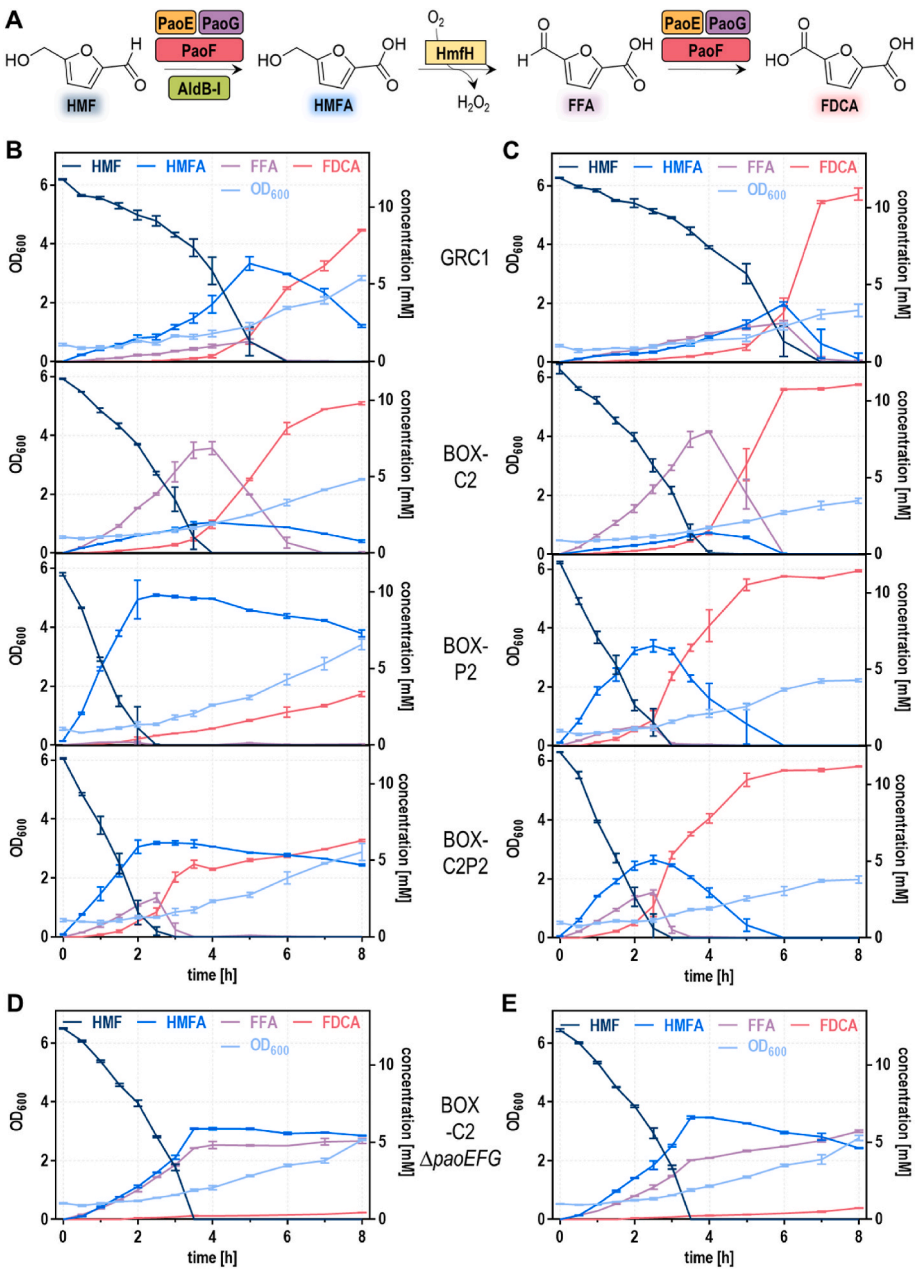

Fig. 5. FDCA production experiments with selected oxidation-optimized BOX-C/P strains. After initial conversion **of** HMF to the respective carboxylic acid HMFA by PaoEFG and AldB-I, two further reaction steps, primary alcohol oxidation to FFA catalyzed by HmfH and a second aldehyde oxidation, are required for FDCA synthesis (**A**). Whole-cell HMF conversion assays in 24-deepwell microplates (two-fold buffered MSM with 40 mM glycerol, 2 mM glucose, and 10 mM HMF) using strains episomally expressing *hmfH* and *hmfT* from plasmids pBT'T_*hmfH* and pJNN_*hmfT* without transporter induction (**A**) and with induction of the transporter by addition of 100 μM salicylate (**B**). Additional experiments under the same conditions with supplementation of 100 μM salicylate were performed with BOX-C2-*hmfH*(g) Δ*paoEFG* (**C**) and BOX-C2-*hmfH-hmfT*(g) Δ*paoEFG* (**D**) underlining the importance of the periplasmic oxidoreductase PaoEFG for FFA oxidation. The mean and standard deviation of three replicates is shown.

enhanced aldehyde conversion on the overall oxidation process. In fact, both BOX-P2-*hmfH-hmfT* and BOX-C2P2-*hmfH-hmfT* achieved complete conversion of 10 mM HMF into 10 mM FDCA 2 h faster than the unmodified control, constituting a 25% increased volumetric rate.

In relative terms, the initial HMF conversion rates remained comparable to those observed for the unmodified BOX-C/P strains, although absolute oxidation rates in these plasmid-harboring strains were reduced overall (Fig. 4B, Fig. S6). This can be attributed to the extra resources required for plasmid maintenance and selection. The strain based on BOX-P2 rapidly accumulated HMFA, whose further conversion by cytoplasmic HmfH seems to be limited by cellular uptake, as suggested by the flattening FDCA concentration curve (Fig. 5C). Expression of *hmfT* alleviated this limitation, making it likely that HMFA is the main substrate of the transporter. Yet, even upon full induction (100 μM salicylate), HMFA was still taken up slower than it was produced, indicating that HMF oxidation in the BOX strains was enhanced to such an extent that HMFA uptake became the rate-limiting reaction. This bottleneck was even more pronounced in a second set of BOX-C/P-*hmfH-hmfT*(g) strains with single copies of the *hmfT* and *hmfH* expression cassettes integrated into the genome, which showed even slower HMFA uptake (Fig. S7). The transport problem could be partly avoided by cytoplasmic HMF oxidation, because overexpression of *aldB-I* in BOX-C2-*hmfH-hmfT* led to transient accumulation of FFA. Increased AldB-I levels resulted in a higher proportion of HMFA formed in the

cytoplasm, where it was directly available for further reaction of the co-localized HmfH. The secreted FFA was rapidly converted to FDCA only once HMF was completely consumed (Fig. 5). This indicates that PaoEFG has a higher affinity for HMF, which competitively inhibits FFA oxidation. BOX-C2P2-*hmfH-hmfT* with maximized HMF oxidation capacity showed a mixed pattern characterized by the accumulation of both FFA and mostly HMFA so that a transport limitation occurred here as well (Fig. 5). Despite this newly emerged challenge, the overall results demonstrated that enhanced HMF oxidation not only increased aldehyde tolerance, but also accelerated FDCA production.

To test whether the HMFA transport limitation could be circumvented by a strain solely relying on boosted cytoplasmic HMF oxidation we deleted *paoEFG* in the BOX-C2 strain. Although periplasmic detoxification was proven crucial for HMF tolerance ensuring a lower intracellular stressor concentration, the colocalization of HMF and HMFA oxidation could alleviate the transport bottleneck. We conducted experiments with the genomically modified BOX-C2-*hmfH-hmfT*(g) Δ*paoEFG* as well as BOX-C2-*hmfH*(g) Δ*paoEFG* lacking the transporter gene (Fig. 5C and D). Surprisingly, FDCA production was almost completely abolished in both cases and FFA accumulated instead. Moreover, despite the absence of periplasmic detoxification, we still detected a large amount of about 5 mM HMFA in every culture broth, which was only further converted slowly in presence of HmfT (Fig. 5D). From this, the following conclusions might be drawn: 1) In BOX-*hmfH-hmfT* strains FFA is almost exclusively oxidized in the periplasm by PaoEFG. Either AldB-I has very low activity towards FFA, or FFA is exported and not taken back up into the cell. 2) The investigated strains are able to secrete HMFA from the cytoplasm, counteracting HmfT-mediated uptake. This probably explains the extracellular accumulation of the acid in previous FDCA production experiments. Incidentally, this also applies to FFA and FDCA as all concentration measurements could be performed without previous cell lysis. 3) In contrast to previous suggestions (Wierckx et al., 2015), HmfT does not contribute to HMF uptake because the initial rates of HMF decrease were virtually identical for BOX-C2-*hmfH-hmfT*(g) Δ*paoEFG* and BOX-C2-*hmfH*(g) Δ*paoEFG* lacking the transporter gene (Fig. 5C and D, Fig. S7). The very high metabolic rates and low hydrophobicity of HMF strongly suggest facilitated uptake, which has not been understood so far. This could explain why Guarnieri et al. had success in engineering *P. putida* KT2440 to grow on HMF and furfural by transplanting the *hmf*-cluster from *Paraburkholderia phytofirmans* without the transporter gene. Besides, they used a medium without molybdenum supplementation, which may have reduced periplasmic oxidation thereby preventing the HMFA uptake issue (Guarnieri et al., 2017).

The new findings prompted us to update the hitherto applied reaction scheme (Wierckx et al., 2015) for biocatalytic conversion of HMF to FDCA by *Pseudomonas* whole-cells (Fig. 6). In addition to the now established enzymes for the aldehyde oxidation steps and their respective cosubstrates, valuable insights into the cellular localization and respective transport routes could be gained. In the BOX strains engineered in this work, HMF oxidation rates are boosted to such an extent, that HMFA uptake becomes the rate-limiting step, even with strong episomal expression of the transporter gene. The uptake mechanism of the substrate HMF as well as the secretion of all furanic compounds from the cytoplasm remain cryptic, and should be the subject of further study.

3. Conclusion and outlook

Aldehydes, such as the emerging renewable platform chemical HMF, are highly toxic for biological systems due to their reactivity. This study revealed the periplasmic PaoEFG and cytoplasmic AldB-I(I) enzymes involved in the oxidative detoxification of HMF by *P. taiwanensis* VLB120 and *P. putida* KT2440. Oxidation-enhanced BOX strains were generated by overexpression of the newly identified genes showing significantly improved tolerance, and HMF oxidation rates up to ten-fold higher than the progenitor GRC1. Thanks to their high oxidative capacity, these strains are perfectly suited for application in whole-cell HMF oxidation processes. The BOX strains also enabled faster FDCA production when equipped with the alcohol oxidase HmfH and the transporter HmfT. To further advance biotechnological FDCA synthesis from HMF, future efforts should focus on HMFA uptake, which emerged as new rate-limiting step in the BOX strains. Besides boosted oxidation, a strain with reduced oxidation and reduction (ROAR) was also constructed which features more than 40-fold slower HMF conversion than GRC1, and even up to 400-fold slower than the best BOX strain. This ROAR strain can serve as valuable platform for a wide range of applications including targeted enzyme engineering for further optimization of HMF oxidation rates and exploration of additional tolerance mechanisms complementing fast aldehyde conversion. If the substrate spectrum of the identified newly identified enzymes extends beyond HMF, the ROAR strain is also an appropriate choice for microbial synthesis of valuable aromatic aldehydes and can serve as an alternative chassis to *E. coli* RARE/ROAR (Butler et al., 2023; Kunjapur et al., 2014), bringing all the advantages of *Pseudomonas* as platform host (Blombach et al., 2022; Nikel et al., 2016; Nikel and de Lorenzo, 2018).

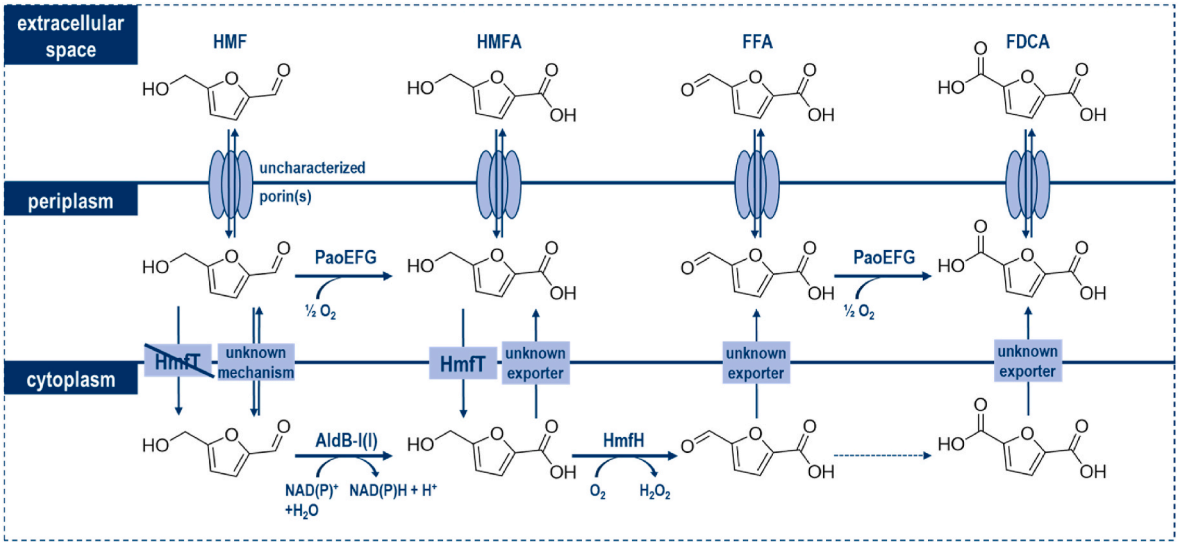

Fig. 6. Updated reaction scheme covering the entire oxidative pathway from HMF to FDCA.

4. Materials and methods

4.1. Strains and culture conditions

For routine cultivation of bacterial strains premixed LB medium containing 10 g L^{-1} peptone, 5 g L^{-1} sodium chloride, and 5 g L^{-1} yeast extract or solid LB with additional 15 g L^{-1} agar (Carl Roth, Karlsruhe, Germany) was applied. All bacterial strains used in this study are listed in Table S3. *Paraburkholderia caribensis* DSM 13236 was acquired from DSMZ (Braunschweig, Germany). To select for *Pseudomonas* after mating procedures LB agar plates were supplemented with irgasan (25 mg L^{-1}). Growth and conversion experiments were conducted in MSM adapted from Hartmans et al. (1989) notably containing $Na_2MoO_4 \times 2H_2O$ at a concentration of 0.2 mg L^{-1}, which was omitted as indicated for experiments involving the transporter deletion mutant GRC1 Δ*modABC*. As carbon sources, a mixture of glycerol (40 mM) and glucose (2 mM) was used. Employing glycerol avoided further acidification of the medium by gluconate, which already occurred through the formation of HMFA as product of oxidative HMF detoxification. Nevertheless, a small amount of glucose was added to prevent an extensive lag phase (Koopman et al., 2010a). The standard buffer capacity (22.3 mM K_2HPO_4 and 13.6 mM NaH_2PO_4) was commonly increased four-fold for HMF conversion assays or as indicated for the respective experiment. For plasmid maintenance and the selection of genomic recombination events the following antibiotics were employed: Kanamycin sulfate at 50 mg L^{-1}, gentamycin sulfate at 20 mg L^{-1}, ampicillin (only for *E. coli*) at 100 mg L^{-1}, and streptomycin sulfate at 50 mg L^{-1} (for *E. coli*) and 200 mg L^{-1} (for *Pseudomonas*). Induction of heterologous gene expression controlled by the *nagR/PnagAa* promoter system was achieved by addition of 0.1 mM salicylate to the MSM preculture and the main experiment. *E. coli* was grown at 37 °C and *Pseudomonas* at 30 °C. Liquid cultures in shake flasks were incubated in a horizontal rotary shaker (Kuhner Shaker, Herzogenrath, Germany) with a humidity of 80%, a throw of 50 mm, and a frequency of 200 rpm. For cultures in 24-deep-well microplates, the frequency was increased to 300 rpm. A Growth Profiler 960 (Enzyscreen, Heemstede, The Netherlands) monitoring cultures in microtiter plates with transparent bottoms by image analysis was used for online growth detection. The resulting green-values (g-values, based on green pixel counts) correlate with the optical density of a cell culture which is sufficient for qualitative statements. No conversion to OD_{600} values was performed, as calibrations depend on cell shape and size, which can vary in the presence of different stressor concentrations. This would require separate calibrations for each specific condition. Main cultures were conducted in 96-well plates (CR1496dg) with a volume of 200 µL at 30 °C and 225 rpm shaking speed with an amplitude of 50 mm. The starting OD_{600} was set to 0.1. The interval between two photos for growth analysis was 30 min. The growth curves displayed were generated by applying a second-order smoothing to all data points. All chemicals used in this study were obtained from Sigma-Aldrich (St. Louis, MO, USA), Carl Roth (Karlsruhe, Germany), or Merck (Darmstadt, Germany) unless stated otherwise.

4.2. Plasmid cloning and strain engineering

Genomic DNA of *P. taiwanensis* VLB120, *P. putida* KT2440 and *P. caribensis* was isolated using the Monarch® Genomic DNA Purification Kit (New England Biolabs, Ipswich, MA, USA). All Plasmids were constructed via Gibson assembly (Gibson et al., 2009) using the NEBuilder HiFi DNA Assembly (New England Biolabs, Ipswich, MA, USA) and verified by Sanger sequencing. Primers were obtained as unmodified DNA oligonucleotides from Eurofins Genomics (Ebersberg, Germany). All oligonucleotides and plasmids used in this study, accompanied by detailed information can be found in Table S4 and Table S5. DNA amplifications for cloning purpose were performed with Q5 High-Fidelity Polymerase (New England Biolabs, Ipswich, MA, USA). Restriction enzymes were purchased from New England Biolabs. Plasmid DNA and PCR amplicons were purified with the Monarch® Plasmid Miniprep Kit and Monarch® PCR & DNA Cleanup Kit, respectively (New England Biolabs, Ipswich, MA, USA). *E. coli* and *Pseudomonas* were transformed with DNA assemblies and purified plasmids by electroporation using a GenePulser Xcell (BioRad, Hercules, CA, USA) (settings: 2 mm cuvette gap, 2.5 kV, 200 Ω, 25 µF). Alternatively, a heat shock protocol was applied in case of *E. coli*. The correctness of cloned plasmids, obtained deletions and integrations, as well as genomic replacements was verified by colony PCR using the OneTaq 2X Master Mix with Standard Buffer (New England Biolabs, Ipswich, MA, USA). To increase efficiency, the template cell material was lysed in alkaline polyethylene glycol according to Chomczynski and Rymaszewski (2006).

Seamless genomic modifications were achieved using the I-SceI-based system developed by Martínez-García and de Lorenzo (Martinez-Garcia and de Lorenzo, 2011). For knockouts, the 500–800 bp upstream and downstream flanking regions of the deletion target (TS1 and TS2) were cloned between the two I-SceI restriction sites of pSNW2, pSNW4, or pEMG, and the resulting plasmid was transferred from *E. coli* PIR2 or *E. coli* EC100D™ *pir*$^+$ into the desired *Pseudomonas* recipient strain by conjugation. For this, mating procedures were performed as described by Wynands et al. (2018). Analogously, precisely positioned genomic integrations or exchanges were carried out with plasmids having the target DNA sequence inserted between the TS sites. Three randomly picked clones were transformed with I-SceI-encoding plasmid pSW-2 triggering the second homologous recombination event without induction by 3-methylbenzoate. Correct clones were cured of pSW-2 by restreaking on non-selective medium, and re-analyzed by PCR ensuring a pure culture. Additional Sanger sequencing verified strains with genomic exchanges such as modified promoter regions.

4.3. Analytical methods

Concentrations of furanic compounds were measured using a 1260 Infinity II HPLC system equipped with an InfinityLab Poroshell 120 EC-C18 column (3.0 × 150 mm, 2.7 µm) column and the respective InfinityLab Poroshell 120 EC-C18 (3.0 × 5 mm, 2.7 µm) guard column (all Agilent, Santa Clara, CA, USA). Chromatography was performed at 40 °C with potassium acetate buffer (10 mM, pH = 5.5) and acetonitrile as eluents at a flow rate of 0.8 mL min^{-1} for 7 min. From the starting ratio of 97% aqueous buffer and 3% acetonitrile the proportion of acetonitrile was first elevated linearly to 15% the first minute and then further increased to 40% the following 2 min. Thereafter, the proportion of acetonitrile remained constant for the next minute before it was gradually reduced to 3% within 2 min and kept constant for the rest of the run. UV detection was performed at distinct wavelengths for each compound: HMF at 280 nm, HMFA at 250 nm, FFA at 280 nm, FDCA at 250 nm, and HMFOH at 220 nm. Retention times were 2.44 min, 0.95 min, 1.14 min, 0.73 min, and 2.28 min for HMF, HMFA, FFA, FDCA, and HMFOH respectively. Standards of each chemical were purchased from Biosynth and used for quantification.

4.4. Whole-cell HMF conversion assays in shake flasks

MSM (10 mL) supplemented with 40 mM glycerol and 2 mM glucose was inoculated using glycerol stocks of the strains to be examined and incubated for approximately 18 h at 30 °C and 200 rpm. Precultures were concentrated by centrifugation (6000×*g*, rt, 5 min) and subsequent resuspension in one fifth of the medium, and used for inoculation of the main experiment. The main culture was carried out in four-fold buffered MSM (10 mL) supplemented with 40 mM glycerol, 2 mM glucose, and 10 mM HMF (30 °C and 200 rpm). The starting OD_{600} was adjusted to 1.0 unless stated otherwise. The first sample was withdrawn directly after inoculation and then in regular intervals. Cell growth was monitored by measuring the optical density at 600 nm and concentrations of respective furanics were analyzed by HPLC. 20 µL of culture broth were diluted ten-fold by addition of 180 µL dH_2O and filtered (AcroPrep™

Advance 96-well, 0,2 μm, PTFE membrane, Pall Corporation, Port Washington, NY, USA). 1 μL of each sample was injected onto the HPLC. The initial conversion rates were defined as the decrease in the concentration of HMF or the increase in the concentration of HMFA normalized to the OD_{600} during the first 2 h of the reaction or until HMF was completely consumed, and determined by linear regression. The OD_{600} was assumed constant during this period and equaled the starting conditions.

4.5. Whole-cell HMF conversion assays in 24-deepwell microplates (Duetz-System)

For parallel analyses of HMF conversion of multiple strains, polypropylene square 24-deepwell microplates capped with a sandwich cover with pins were employed (Enzyscreen, Heemstede, Netherlands). Cells used for inoculation of the main experiment were obtained as described above with an additional first passage in LB medium. The main culture was carried out in four-fold buffered MSM (1.5 mL) supplemented with 40 mM glycerol, 2 mM glucose, and 10 mM HMF (30 °C and 300 rpm). The starting OD_{600} was adjusted to 0.5 unless stated otherwise. Samples were taken in regular intervals of 30 min, which were prolonged to 1 h after 4 h of experiment (Sampling interval was shortened in case of fast-oxidizing strains). For each time point, a separate microplate was harvested. Measurements of cell growth and furanics concentrations, as well as determination of initial oxidation rates were carried out as described in the previous section.

Funding

This work was supported by the German Federal Ministry of Education and Research via the project NO-STRESS [grant number 031B0852A] and by the European Union's Horizon 2020 research and innovation program via the project UPLIFT [grant agreement number 953073].

CRediT authorship contribution statement

Thorsten Lechtenberg: Investigation, Validation, Visualization, Writing – original draft, Writing – review & editing. **Benedikt Wynands:** Conceptualization, Supervision, Writing – review & editing. **Nick Wierckx:** Conceptualization, Funding acquisition, Project administration, Supervision, Writing – review & editing.

Declaration of competing interest

The authors declare no competing interests.

Data availability

Data will be made available on request.

Acknowledgements

We thank R. Schruff for her support with generating the deletion mutants of *P. putida* KT2440 and Pablo I. Nikel for kindly providing the pSNW2 and pSNW4 plasmids.

Appendix A. Supplementary data

Supplementary data to this article can be found online at https://doi.org/10.1016/j.ymben.2023.12.010.

References

Achouak, W., Christen, R., Barakat, M., Martel, M.H., Heulin, T., 1999. Burkholderia caribensis sp. nov., an exopolysaccharide-producing bacterium isolated from vertisol microaggregates in Martinique. Int. J. Syst. Bacteriol. 49, 787–794.

Adewunmi, Y., Namjilsuren, S., Walker, W.D., Amato, D.N., Amato, D.V., Mavrodi, O.V., Patton, D.L., Mavrodi, D.V., 2020. Antimicrobial activity of, and cellular pathways targeted by, p-anisaldehyde and epigallocatechin gallate in the opportunistic human pathogen Pseudomonas aeruginosa. Appl. Environ. Microbiol. 86.

Bitzenhofer, N.L., Kruse, L., Thies, S., Wynands, B., Lechtenberg, T., Rönitz, J., Kozaeva, E., Wirth, N.T., Eberlein, C., Jaeger, K.E., Nikel, P.I., Heipieper, H.J., Wierckx, N., Loeschcke, A., 2021. Towards robust Pseudomonas cell factories to harbour novel biosynthetic pathways. Essays Biochem. 65, 319–336.

Blombach, B., Grunberger, A., Centler, F., Wierckx, N., Schmid, J., 2022. Exploiting unconventional prokaryotic hosts for industrial biotechnology. Trends Biotechnol. 40, 385–397.

Bozell, J.J., Petersen, G.R., 2010. Technology development for the production of biobased products from biorefinery carbohydrates—the US Department of Energy's "Top 10" revisited. Green Chem. 12.

Butler, N.D., Anderson, S.R., Dickey, R.M., Nain, P., Kunjapur, A.M., 2023. Combinatorial gene inactivation of aldehyde dehydrogenases mitigates aldehyde oxidation catalyzed by E. coli resting cells. Metab. Eng. 77, 294–305.

Chomczynski, P., Rymaszewski, M., 2006. Alkaline polyethylene glycol-based method for direct PCR from bacteria, eukaryotic tissue samples, and whole blood. Biotechniques 40 (454), 456–458.

Correia, M.A.S., Otrelo-Cardoso, A.R., Schwuchow, V., Clauss, K.G.V.S., Haumann, M., Romao, M.J., Leimkuhler, S., Santos-Silva, T., 2016. The Escherichia coli periplasmic aldehyde oxidoreductase is an exceptional member of the xanthine oxidase family of molybdoenzymes. ACS Chem. Biol. 11, 2923–2935.

Davidson, M.G., Elgie, S., Parsons, S., Young, T.J., 2021. Production of HMF, FDCA and their derived products: a review of life cycle assessment (LCA) and techno-economic analysis (TEA) studies. Green Chem. 23, 3154–3171.

de Avila, E.S.S., Echeverrigaray, S., Gerhardt, G.J., 2011. BacPP: bacterial promoter prediction–a tool for accurate sigma-factor specific assignment in enterobacteria. J. Theor. Biol. 287, 92–99.

Doi, S., Hashimoto, Y., Tomita, C., Kumano, T., Kobayashi, M., 2016. Discovery of piperonal-converting oxidase involved in the metabolism of a botanical aromatic aldehyde. Sci. Rep. 6, 38021.

Galkin, K.I., Ananikov, V.P., 2019. When will 5-hydroxymethylfurfural, the "sleeping giant" of sustainable chemistry, awaken? ChemSusChem 12, 2976–2982.

Garcia-Hidalgo, J., Brink, D.P., Ravi, K., Paul, C.J., Liden, G., Gorwa-Grauslund, M.F., 2020. Vanillin production in Pseudomonas: whole-genome sequencing of Pseudomonas sp. strain 9.1 and reannotation of Pseudomonas putida CaIA as a vanillin reductase. Appl. Environ. Microbiol. 86.

Gibson, D.G., Young, L., Chuang, R.Y., Venter, J.C., Hutchison, C.A., Smith, H.O., 2009. Enzymatic assembly of DNA molecules up to several hundred kilobases. Nat. Methods 6, 343. U41.

Graf, N., Altenbuchner, J., 2014. Genetic engineering of Pseudomonas putida KT2440 for rapid and high-yield production of vanillin from ferulic acid. Appl. Microbiol. Biotechnol. 98, 137–149.

Guarnieri, M.T., Ann Franden, M., Johnson, C.W., Beckham, G.T., 2017. Conversion and assimilation of furfural and 5-(hydroxymethyl)furfural by Pseudomonas putida KT2440. Metab Eng Commun 4, 22–28.

Hartmans, S., Smits, J.P., van der Werf, M.J., Volkering, F., de Bont, J.A., 1989. Metabolism of styrene oxide and 2-phenylethanol in the styrene-degrading xanthobacter strain 124X. Appl. Environ. Microbiol. 55, 2850–2855.

Heer, D., Sauer, U., 2008. Identification of furfural as a key toxin in lignocellulosic hydrolysates and evolution of a tolerant yeast strain. Microb. Biotechnol. 1, 497–506.

Hossain, G.S., Yuan, H., Li, J., Shin, H.-D., Wang, M., Du, G., Chen, J., Liu, L., 2017. Metabolic engineering of Raoultella ornithinolytica BF60 for production of 2,5-furandicarboxylic acid from 5-hydroxymethylfurfural. Appl. Environ. Microbiol. 83. AEM.02312-16.

Hsu, C.T., Kuo, Y.C., Liu, Y.C., Tsai, S.L., 2020. Green conversion of 5-hydroxymethylfurfural to furan-2,5-dicarboxylic acid by heterogeneous expression of 5-hydroxymethylfurfural oxidase in Pseudomonas putida S12. Microb. Biotechnol. 13, 1094–1102.

Kim, H.S., Choi, J.A., Kim, B.Y., Ferrer, L., Choi, J.M., Wendisch, V.F., Lee, J.H., 2022. Engineered Corynebacterium glutamicum as the platform for the production of aromatic aldehydes. Front. Bioeng. Biotechnol. 10.

Koopman, F., Wierckx, N., de Winde, J.H., Ruijssenaars, H.J., 2010a. Efficient whole-cell biotransformation of 5-(hydroxymethyl)furfural into FDCA, 2,5-furandicarboxylic acid. Bioresour. Technol. 101, 6291–6296.

Koopman, F., Wierckx, N., de Winde, J.H., Ruijssenaars, H.J., 2010b. Identification and characterization of the furfural and 5-(hydroxymethyl)furfural degradation pathways of Cupriavidus basilensis HMF14. Proc. Natl. Acad. Sci. U. S. A. 107, 4919–4924.

Kozono, I., Hibi, M., Takeuchi, M., Ogawa, J., 2020. Purification and characterization of molybdenum-containing aldehyde dehydrogenase that oxidizes benzyl maltol derivative from Pseudomonas nitroreducens SB32154. Biosc. Biotech. Biochem. 84, 2390–2400.

Kunjapur, A.M., Prather, K.L.J., 2015. Microbial engineering for aldehyde synthesis. Appl. Environ. Microbiol. 81, 1892–1901.

Kunjapur, A.M., Tarasova, Y., Prather, K.L.J., 2014. Synthesis and accumulation of aromatic aldehydes in an engineered strain of Escherichia coli. J. Am. Chem. Soc. 136, 11644–11654.

Lee, C., Park, C., 2017. Bacterial responses to glyoxal and methylglyoxal: reactive electrophilic species. Int. J. Mol. Sci. 18.
Li, W.J., Narancic, T., Kenny, S.T., Niehoff, P.J., O'Connor, K., Blank, L.M., Wierckx, N., 2020. Unraveling 1,4-butanediol metabolism in Pseudomonas putida KT2440. Front. Microbiol. 11.
Lin, T.Y., Wen, R.C., Shen, C.R., Tsai, S.L., 2020. Biotransformation of 5-hydroxymethylfurfural to 2,5-furandicarboxylic acid by a syntrophic consortium of engineered synechococcus elongatus and Pseudomonas putida. Biotechnol. J. 15, 1900357.
Liu, P., Xie, J., Tan, H., Zhou, F., Zou, L., Ouyang, J., 2020. Valorization of Gelidium amansii for dual production of D-galactonic acid and 5-hydroxymethyl-2-furancarboxylic acid by chemo-biological approach. Microb. Cell Factories 19, 104.
Loos, K., Zhang, R., Pereira, I., Agostinho, B., Hu, H., Maniar, D., Sbirrazzuoli, N., Silvestre, A.J.D., Guigo, N., Sousa, A.F., 2020. A perspective on PEF synthesis, properties, and end-life. Front. Chem. 8, 585.
LoPachin, R.M., Gavin, T., 2014. Molecular mechanisms of aldehyde toxicity: a chemical perspective. Chem. Res. Toxicol. 27, 1081–1091.
Martinez-Garcia, E., de Lorenzo, V., 2011. Engineering multiple genomic deletions in Gram-negative bacteria: analysis of the multi-resistant antibiotic profile of Pseudomonas putida KT2440. Environ. Microbiol. 13, 2702–2716.
McKenna, S.M., Mines, P., Law, P., Kovacs-Schreiner, K., Birmingham, W.R., Turner, N. J., Leimkuhler, S., Carnell, A.J., 2017. The continuous oxidation of HMF to FDCA and the immobilisation and stabilisation of periplasmic aldehyde oxidase (PaoABC). Green Chem. 19, 4660–4665.
Mukhopadhyay, A., 2015. Tolerance engineering in bacteria for the production of advanced biofuels and chemicals. Trends Microbiol. 23, 498–508.
Mutalik, V.K., Guimaraes, J.C., Cambray, G., Lam, C., Christoffersen, M.J., Mai, Q.A., Tran, A.B., Paull, M., Keasling, J.D., Arkin, A.P., Endy, D., 2013. Precise and reliable gene expression via standard transcription and translation initiation elements. Nat. Methods 10, 354–360.
Neumann, M., Mittelstadt, G., Iobbi-Nivol, C., Saggu, M., Lendzian, F., Hildebrandt, P., Leimkuhler, S., 2009. A periplasmic aldehyde oxidoreductase represents the first molybdopterin cytosine dinucleotide cofactor containing molybdo-flavoenzyme from Escherichia coli. FEBS J. 276, 2762–2774.
Nikel, P.I., Chavarria, M., Danchin, A., de Lorenzo, V., 2016. From dirt to industrial applications: Pseudomonas putida as a Synthetic Biology chassis for hosting harsh biochemical reactions. Curr. Opin. Chem. Biol. 34, 20–29.
Nikel, P.I., de Lorenzo, V., 2018. Pseudomonas putida as a functional chassis for industrial biocatalysis: from native biochemistry to trans-metabolism. Metab. Eng. 50, 142–155.
Pham, N.N., Chen, C.Y., Li, H., Nguyen, M.T.T., Nguyen, P.K.P., Tsai, S.L., Chou, J.Y., Ramli, T.C., Hu, Y.C., 2020. Engineering stable Pseudomonas putida S12 by CRISPR for 2,5-furandicarboxylic acid (FDCA) production. ACS Synth. Biol. 9, 1138–1149.
Sayed, M., Gaber, Y., Junghus, F., Martín, E.V., Pyo, S.H., Hatti-Kaul, R., 2022. Oxidation of 5-hydroxymethylfurfural with a novel aryl alcohol oxidase from Mycobacterium sp. MS1601. Microb. Biotechnol. 15, 2176–2190.
Sheng, Y., Tan, X., Zhou, X., Xu, Y., 2020. Bioconversion of 5-hydroxymethylfurfural (HMF) to 2,5-furandicarboxylic acid (FDCA) by a native obligate aerobic bacterium, acinetobacter calcoaceticus NL14. Appl. Biochem. Biotechnol. 192, 455–465.
Tan, H., Zhou, F., Liao, D., Ouyang, J., Zheng, Z., 2020. Improved biosynthesis of 2,5-Furandicarboxylic acid through coupling of heterologous pathways in Escherichia coli and native pathways in Pseudomonas putida. Biochem. Eng. J. 161, 107657.
Troiano, D., Orsat, V., Dumont, M.J., 2020. Status of biocatalysis in the production of 2,5-furandicarboxylic acid. ACS Catal. 10, 9145–9169.
van Putten, R.J., van der Waal, J.C., de Jong, E., Rasrendra, C.B., Heeres, H.J., de Vries, J.G., 2013. Hydroxymethylfurfural, a versatile platform chemical made from renewable resources. Chem. Rev. 113, 1499–1597.
Wang, H.Y., Li, Q., Kuang, X.L., Xiao, D.F., Han, X.B., Hu, X.D., Li, X., Ma, M.G., 2018. Functions of aldehyde reductases from Saccharomyces cerevisiae in detoxification of aldehyde inhibitors and their biotechnological applications. Appl. Microbiol. Biotechnol. 102, 10439–10456.
Wehrmann, M., Elsayed, E.M., Köbbing, S., Bendz, L., Lepak, A., Schwabe, J., Wierckx, N., Bange, G., Klebensberger, J., 2020. An engineered PQQ-dependent alcohol dehydrogenase for the oxidation of 5-(hydroxymethyl)furoic acid. ACS Catal. 10, 7836–7842.
Wierckx, N., Elink Schuurman, T.D., Blank, L.M., Ruijssenaars, H.J., 2015. Whole-cell biocatalytic production of 2,5-furandicarboxylic acid. Microorganisms in Biorefineries, pp. 207–223.
Wierckx, N., Koopman, F., Ruijssenaars, H.J., de Winde, J.H., 2011. Microbial degradation of furanic compounds: biochemistry, genetics, and impact. Appl. Microbiol. Biotechnol. 92, 1095–1105.
Winsor, G.L., Griffiths, E.J., Lo, R., Dhillon, B.K., Shay, J.A., Brinkman, F.S., 2016. Enhanced annotations and features for comparing thousands of Pseudomonas genomes in the Pseudomonas genome database. Nucleic Acids Res. 44, D646–D653.
Wu, Q., Zong, M.H., Li, N., 2023. One-pot chemobiocatalytic production of 2,5-Bis (hydroxymethyl)furan and its diester from biomass in aqueous media. ACS Catal. 13, 9404–9414.
Wynands, B., Lenzen, C., Otto, M., Koch, F., Blank, L.M., Wierckx, N., 2018. Metabolic engineering of Pseudomonas taiwanensis VLB120 with minimal genomic modifications for high-yield phenol production. Metab. Eng. 47, 121–133.
Wynands, B., Otto, M., Runge, N., Preckel, S., Polen, T., Blank, L.M., Wierckx, N., 2019. Streamlined Pseudomonas taiwanensis VLB120 chassis strains with improved bioprocess features. ACS Synth. Biol. 8, 2036–2050.
Xu, C., Paone, E., Rodriguez-Padron, D., Luque, R., Mauriello, F., 2020a. Recent catalytic routes for the preparation and the upgrading of biomass derived furfural and 5-hydroxymethylfurfural. Chem. Soc. Rev. 49, 4273–4306.
Xu, Q., Zheng, Z., Zou, L., Zhang, C., Yang, F., Zhou, K., Ouyang, J., 2020b. A versatile Pseudomonas putida KT2440 with new ability: selective oxidation of 5-hydroxymethylfurfural to 5-hydroxymethyl-2-furancarboxylic acid. Bioproc. Biosyst. Eng. 43, 67–73.
Yuan, H., Liu, H., Du, J., Liu, K., Wang, T., Liu, L., 2020. Biocatalytic production of 2,5-furandicarboxylic acid: recent advances and future perspectives. Appl. Microbiol. Biotechnol. 104, 527–543.
Yuan, H., Liu, Y., Lv, X., Li, J., Du, G., Shi, Z., Liu, L., 2018. Enhanced 2,5-furandicarboxylic acid (FDCA) production in RaoultellaornithinolyticaBF60 by manipulation of the key genes in FDCA biosynthesis pathway. J. Microbiol. Biotechnol. 28, 1999–2008.
Zheng, Z., Xu, Q., Tan, H., Zhou, F., Ouyang, J., 2020. Selective biosynthesis of furoic acid from furfural by Pseudomonas putida and identification of molybdate transporter involvement in furfural oxidation. Front. Chem. 8, 587456.
Zhou, J., Chen, Z., Wang, Y., 2020. Bioaldehydes and beyond: expanding the realm of bioderived chemicals using biogenic aldehydes as platforms. Curr. Opin. Chem. Biol. 59, 37–46.
Zobel, S., Benedetti, I., Eisenbach, L., de Lorenzo, V., Wierckx, N., Blank, L.M., 2015. Tn7-Based device for calibrated heterologous gene expression in Pseudomonas putida. ACS Synth. Biol. 4, 1341–1351.
Zou, L., Zheng, Z., Tan, H., Xu, Q., Ouyang, J., 2020. Synthesis of 2,5-furandicarboxylic acid by a TEMPO/laccase system coupled with Pseudomonas putida KT2440. RSC Adv. 10, 21781–21788.